Title	Selective Anion Manipulation for Controlling the Thermoelectric Properties of Epitaxial SnO2 Films on r-Al2O3
Author(s)	Ishibe, Takafumi; Kozuki, Seiya; Komatsubara, Yuki et al.
Citation	ACS Applied Energy Materials. 2025, 8(7), p. 4411-4417
Version Type	AM
URL	https://hdl.handle.net/11094/101046
rights	The full-text file will be made open to the public on 21 March 2026 in accordance with the publisher's policy.
Note	

The University of Osaka Institutional Knowledge Archive : OUKA

https://ir.library.osaka-u.ac.jp/

The University of Osaka

Supporting Information for

Selective Anion Manipulation for Controlling Thermoelectric Properties of Epitaxial SnO_2 Films on r-Al_2O_3

*Takafumi Ishibe[1], Seiya Kozuki[1], Yuki Komatsubara[1], Yuto Uematsu[1], Takashi Yoshizaki[1], Yuichiro Yamashita[2], Nobuyasu Naruse[3], Yutaka Mera[3], Eiichi Kobayashi[4], and Yoshiaki Nakamura[1] **

1 Graduate School of Engineering Science, Osaka University, 1-3 Machikaneyama-cho, Toyonaka, Osaka 560-8531, Japan

2 National Institute of Advanced Industrial Science and Technology, 1-1-1 Umezono, Tsukuba, Ibaraki 305-8563, Japan

3 Department of Fundamental Bioscience, Shiga University of Medical Science, Otsu, Shiga 520-2192, Japan

4 Kyushu Synchrotron Light Research Center, 8-7 Yayoigaoka, Tosu, Saga 841-0005, Japan

**Corresponding author: nakamura.yoshiaki.es@osaka-u.ac.jp*

(Previous address: nakamura@ee.es.osaka-u.ac.jp)

S1 Sample information

Epitaxial SnO_2 films/r-Al_2O_3 substrates were grown using pulsed laser deposition (PLD). Chemically cleaned r-Al_2O_3 substrates were introduced into PLD chamber at a base pressure of ~1×10^{-6} Pa. SnO_2 films were deposited on the substrates by irradiating undoped SnO_2 target using ArF laser (laser wavelength: 193 nm, laser energy: 20 mJ, repetition frequency: 10 Hz, oxygen partial pressure: 5 Pa). The undoped SnO_2 target was fabricated by pressing undoped SnO_2 powder (99.99 %) at 8 MPa and sintering the pressed SnO_2 tablet at 1673 K for 24 hours. The epitaxial SnO_2 films were doped using Arsenic (As) implantation at the accelerated voltage of 72 keV. Then, the dose amount of As was 2×10^{13}-2×10^{15} cm^{-2}. The As dopant was activated by annealing the samples at ~873 K for 10 min in rapid thermal annealing system.

The thickness of doped SnO_2 layer was determined from the As ion distribution profile as a function of depth, the distance from the film surface (Figure S1a). This distribution profile was calculated by stopping and range of ions in matter (SRIM). The distribution profile was fitted with Gaussian function. From the fitted Gaussian function, the integration of implanted ion concentration was calculated (Figure S1b). The integration of implanted ion concentration saturated (99.5 %) at a certain depth (58 nm). We defined the thickness of As-implanted SnO_2 layer as the depth corresponding to the 99.5 % of the integration of implanted ion concentration. The estimation detail is described in our previous studies [1, 2].

The sample information of As-implanted SnO_2 films (As-implanted samples) such as dose amount, carrier concentration n, electron mobility μ, electrical conductivity σ, Seebeck coefficient S, and $S^2\sigma$ are summarized in Table S1.

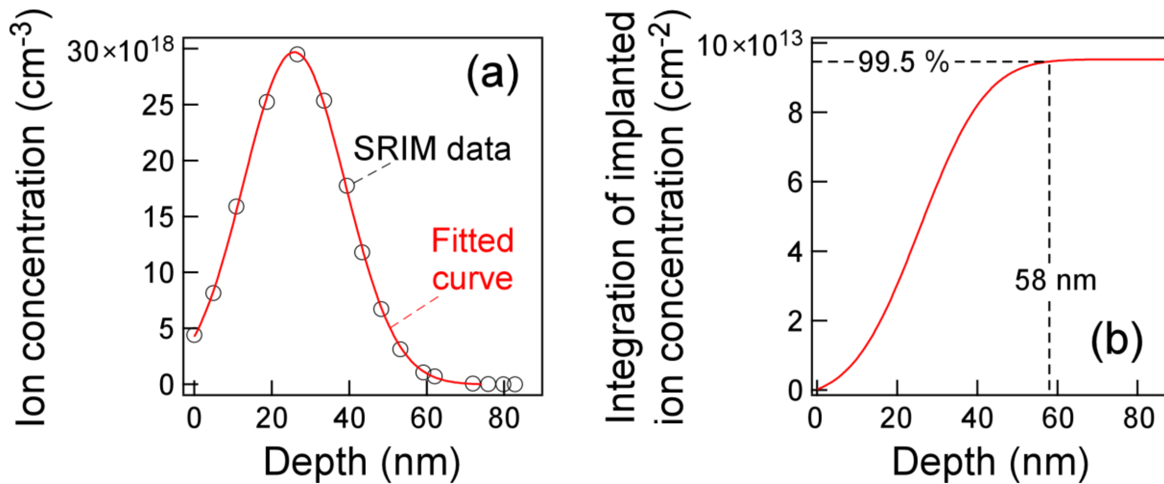

Figure S1(a) As ion implantation profile as a function of depth in the dose amount of 1×10^{14} cm^{-2}, which was calculated using SRIM. The open circles and the solid curve are SRIM data and fitted Gaussian function, respectively. (b) Integration of implanted ion concentration as a function of depth.

Table S1 Sample information at 300 K.

Sample number	Dose amount (cm^{-2})	n (cm^{-3})	μ ($cm^2V^{-1}s^{-1}$)	σ ($\Omega^{-1}cm^{-1}$)	S (μVK^{-1})	$S^2\sigma$ ($\mu Wcm^{-1}K^{-2}$)
1	2×10^{13}	$1.6\pm0.2\times10^{19}$	17.7±2.2	45±0	-199±14	1.8±0.1
2	1×10^{14}	$3.1\pm0.4\times10^{19}$	22.2±2.8	111±0	-140±10	2.2±0.2
3	1×10^{14}	$3.3\pm0.4\times10^{19}$	24.4±3.1	129±0	-151±11	2.9±0.2
4	1×10^{14}	$3.8\pm0.4\times10^{19}$	15.8±2.0	96±0	-152±11	2.2±0.2
5	1×10^{14}	$5.8\pm0.7\times10^{19}$	15.7±2.0	145±0	-131±9	2.5±0.1
6	2×10^{14}	$7.4\pm0.9\times10^{19}$	11.6±1.5	138±0	-118±8	1.9±0.1
7	8×10^{14}	$5.5\pm0.7\times10^{19}$	7.0±0.9	62±0	-104±7	0.7±0.0
8	2×10^{15}	$2.7\pm0.3\times10^{19}$	13.7±1.7	58±0	-119±8	0.8±0.0

S2 Thermal conductivity measurement for As-implanted samples

Thermal conductivities κ of As-implanted samples were measured by 2ω method. Figure S2a shows the typical measurement data of As-implanted samples (dose amount: 1×10^{14} cm^{-2}). Phase signals were fitted with the theoretical equation for surface temperature T_0 of transducer film (eqs (S1)-(S7)). This is derived from the one-dimensional heat conduction model. When obtaining eqs (S1)-(S7), we considered 4 layer model (Figure S2b) under the adiabatic assumption for the surface of transducer film and the bottom of substrate.

$$T_0=\frac{Q}{i\omega C_1}\left(1-\frac{1}{a_1}\frac{1}{1+R_{12}\kappa_1 k_1 t_1+\gamma\beta_{12}t_1}\right) \quad \text{(S1)},$$

$$\gamma=\frac{t_2+R_{23}\kappa_2 k_2+\alpha\beta_{23}}{1+R_{23}\kappa_2 k_2 t_2+\alpha\beta_{23}t_2} \quad \text{(S2)},$$

$$\alpha=\frac{t_3 t_4+R_{34}\kappa_3 k_3 t_4+\beta_{34}}{t_4+R_{34}\kappa_3 k_3 t_3 t_4+\beta_{34}t_3} \quad \text{(S3)},$$

$$a_n=\cosh(k_n d_n) \quad \text{(S4)},$$

$$t_n=\tanh(k_n d_n) \quad \text{(S5)},$$

$$\beta_{nm}=\{\kappa_n C_n/(\kappa_m C_m)\}^{1/2} \quad \text{(S6)},$$

$$k_n=\{\omega C_n/(2\kappa_n)\}^{1/2}(1+i) \quad \text{(S7)},$$

where Q is the Joule heat generated per unit volume in the metallic transducer film, ω is the angular frequency of heating current, κ_n is the κ of the nth layer, d_n is the film thickness of the nth layer, C_n is the volumetric heat capacity of the nth layer, and R_{nm} is the interfacial thermal resistance between the nth and the mth layer. The indices n and m describe the layer: 1 for Mo transducer film; 2 for As-implanted SnO_2 layer; 3 for undoped SnO_2 layer; 4 for Al_2O_3 substrate. The fixed parameters used for the fitting analysis are shown in Table S2. The R_{12} and the R_{34} were measured by time domain thermoreflectance method. The R_{23} was considered to be zero because this interface is formed by homojunction.

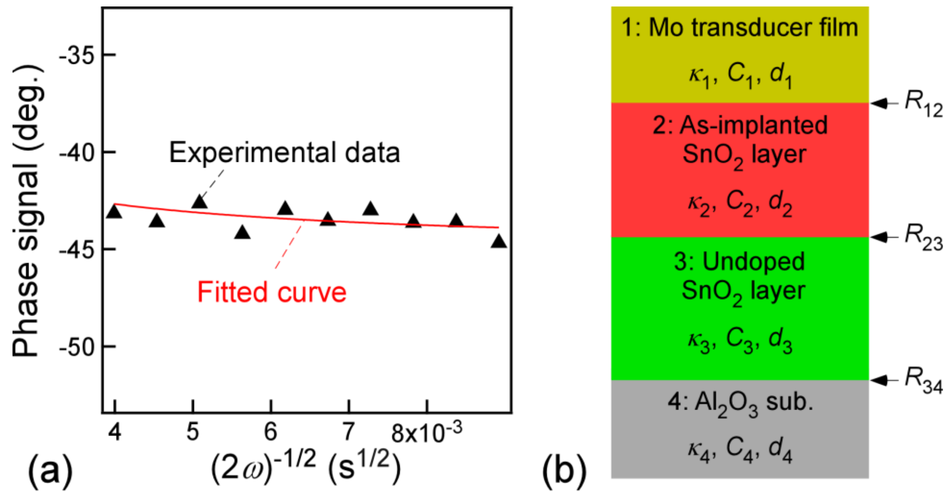

Figure S2(a) Typical 2ω data of As-doped samples with the dose amount of 1×10^{14} cm^{-2}. (b) Schematic illustration of the sample structure.

Table S2 Typical parameters used for fitting analysis in As-doped samples with the dose amount of 1×10^{14} cm^{-2}.

Parameters	unit	Value
κ_1	$Wm^{-1}K^{-1}$	142
C_1	$JK^{-1}m^{-3}$	2.6×10^{6}
d_1	m	2.3×10^{-7}
κ_2	$Wm^{-1}K^{-1}$	fitting parameter
C_2	$JK^{-1}m^{-3}$	2.5×10^{6}
d_2	m	5.8×10^{-8}
κ_3	$Wm^{-1}K^{-1}$	11
C_3	$JK^{-1}m^{-3}$	2.5×10^{6}
d_3	m	5.2×10^{-8}
κ_4	$Wm^{-1}K^{-1}$	27
C_4	$JK^{-1}m^{-3}$	2.3×10^{6}
d_4	m	5.0×10^{-4}
R_{12}	m^2KW^{-1}	3.0×10^{-9}
R_{23}	m^2KW^{-1}	0
R_{34}	m^2KW^{-1}	0

S3 X-ray photoelectron spectroscopy analysis

To analyze the composition and the defect formation, we carried out x-ray photoelectron spectroscopy (XPS) measurements for As-implanted sample with the dose amount of 1×10^{14} cm^{-2} and Sb-doped sample with the dopant amount of 0.2 at%. The XPS measurement was performed using Al K_{α} line (1486.6 eV) after removing the contribution of hydroxyl groups on the sample surfaces by Ar ion sputtering with the energy of 500 V for 3 min. From the wide scan (not shown here), the O/Sn atomic ratios of As-implanted and Sb-doped films were both measured to be ~1.9 roughly although we have difficulty in detecting the difference of the two ratios (<several %) by XPS. This value is close to the stoichiometry of SnO_2 with O/Sn=2.0. Figures S3a and b show O1s XPS spectra of As-implanted and Sb-doped samples, respectively. The preceding studies about XPS spectra of SnO_2 reported that XPS spectra coming from O atoms bounded to tin atoms (O_I) and O vacancies (O_{II}) appeared at the binding energies of ~530-531 and ~531-532 eV, respectively [3-5]. O1s XPS spectra of As-implanted sample and Sb-doped sample were deconvoluted into O_I and O_{II} peaks using voigt function after removing the background using Shirley method, where the best values of the coefficients were the ones that minimize the value of Chi-square. The rate of O_{II} to O_I of As-implanted sample (0.16) was larger than that of Sb-doped sample (0.04). This indicates that As-implanted samples have a larger number of O vacancies than Sb-doped sample, which is consistent with the result of Raman spectroscopy in the main text.

In addition, we measured Sn3d XPS spectra of As-implanted and Sb-doped samples to investigate the influence of O vacancies on the Sn state (Figure S4). Both spectra completely overlapped. This proves that the Sn state was not altered by O vacancy formation.

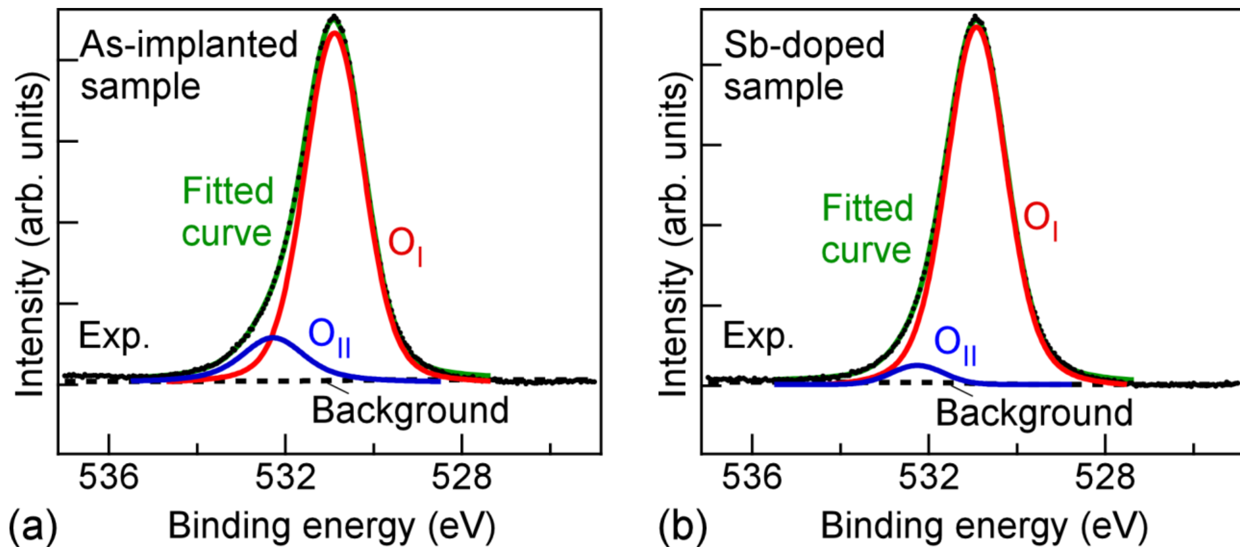

Figure S3(a, b) O1s XPS spectra of As-implanted sample (a) and Sb-doped sample (b).

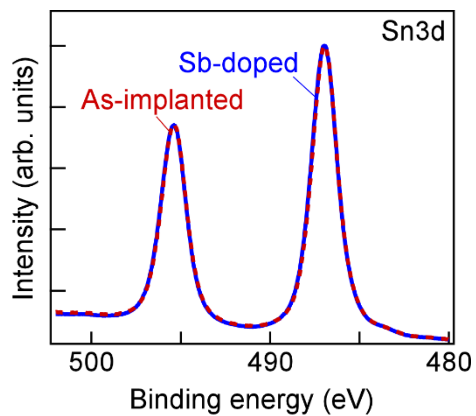

Figure S4 Sn3d XPS spectra of As-implanted (the broken line) and Sb-doped SnO_2 films (the solid line).

S4 Temperature dependences of thermoelectric properties

We show temperature T dependences of S and σ of As-implanted samples (n~3×10^{19} cm^{-3}) and those of Sb-doped samples (n~1×10^{19} cm^{-3}) [6], as shown in Figure S5.

In the case of As-implanted samples, undoped SnO_2 layer may contribute to electrical conduction. Therefore, we removed the contribution of undoped SnO_2 layer on the basis of parallel conduction model; $G_{measure}=G_{As\text{-}imp}+G_{undoped}$ and $S_{measure}(G_{As\text{-}imp}+G_{undoped})=(S_{As\text{-}imp}G_{As\text{-}imp}+S_{undoped}G_{undoped})$, where $S_{measure}$ and $G_{measure}$ are the measured Seebeck coefficient and the measured sheet electrical conductivity, respectively, and $S_{As\text{-}imp}$ ($G_{As\text{-}imp}$) and $S_{undoped}$ ($G_{undoped}$) are Seebeck coefficients (sheet electrical conductivities) of As-implanted SnO_2 layer and undoped SnO_2 layer, respectively. $S_{undoped}$ and $G_{undoped}$ are the measured values of undoped epitaxial SnO_2 film/r-Al_2O_3.

We estimated $S_{As\text{-}imp}$ and $G_{As\text{-}imp}$ on the basis of parallel conduction model using the results of $S_{measure}$, $G_{measure}$, $S_{undoped}$, and $G_{undoped}$. As a result, $S_{As\text{-}imp}$ (the solid squares) were almost equal to $S_{measure}$ (the cross marks) (Figure S5a). $G_{As\text{-}imp}$ were also almost equal to $G_{measure}$; Figure S5a shows that the electrical conductivities of As-implanted SnO_2 layer $\sigma_{As\text{-}imp}$ (the solid circles) were almost equal to the measured electrical conductivities $\sigma_{measure}$ (the open diamonds).

The $\sigma_{As\text{-}imp}$ values were lower than the σ values of the Sb-doped SnO_2 films in the entire T range. This is attributed to mobility reduction coming from effective mass increase. On the other hand, $S_{As\text{-}imp}$ values were almost equal to S values of the Sb-doped SnO_2 films in the entire T range although n of As-implanted samples at room temperature was larger than that of Sb-doped samples. This can also be explained by effective mass increase. Although $S^2\sigma$ of As-implanted samples were slightly lower than those of Sb-doped samples, $S^2\sigma$ of As-implanted samples were kept to be high in the entire T range (Figure S5b) by maintained high S related to effective mass increase.

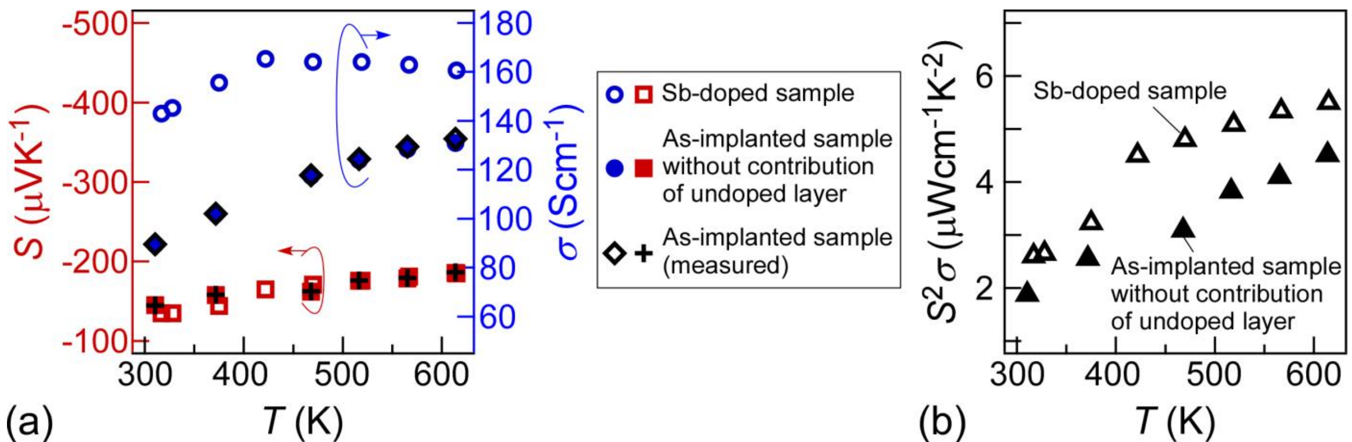

Figure S5 (a, b) T dependences of S (a), σ (b) in Sb-doped samples and As-implanted samples with the dose amount of 1×10^{14} cm^{-2} with and without contribution of undoped layer. In (a), the solid circles (the open circles) and the solid squares (the open squares) are $S_{As\text{-}imp}$ (S of Sb-doped samples) and $\sigma_{As\text{-}imp}$ (σ of Sb-doped samples), respectively. The open diamonds and the cross marks are $\sigma_{measure}$ and $S_{measure}$, respectively. In (b), the open and the solid triangles are $S^2\sigma$ of Sb-doped samples and As-implanted samples with the dose amount of 1×10^{14} cm^{-2} without contribution of undoped layer, respectively.

S5 Calculation of Lorenz number

Lorenz number L was calculated on the basis of Boltzmann transport theory under relaxation time approximation and single parabolic band approximation with density-of-states effective mass m_d of $0.38m_0$ (m_0 is free electron mass) [7] as follows;

$$L=\frac{1}{(qT)^2}\frac{K_0K_2\text{-}K_1^2}{K_0^2} \quad \text{(S8)}.$$

In eq (S8), K_ν (ν=0, 1, 2) is described as follows;

$$K_\nu=\int_0^\infty \Lambda(\xi)(\xi\text{-}\xi_F)^\nu g(\xi)\left(-\frac{\partial f(\xi)}{\partial \xi}\right)\xi \mathrm{d}\xi \quad \text{(S9)},$$

where ξ is reduced energy of carrier, ξ_F is reduced Fermi energy of carrier, $\tau_c(\xi)$ is carrier relaxation time, $g(\xi)$ is carrier density-of-states, and $f(\xi)$ is Fermi-Dirac distribution function. The $\tau_c(\xi)$ can be assumed to be proportional to $\xi^{3/2}$ because the ionized impurity scattering process mainly contributes to carrier transport, as shown in Figure 4c in the main text. From eqs (S8) and (S9), we calculated the theoretical n-L curve at T=300 K. Figure S6 shows the calculated L as a function of n. The electronic thermal conductivity κ_{el} was calculated using this n-L curve.

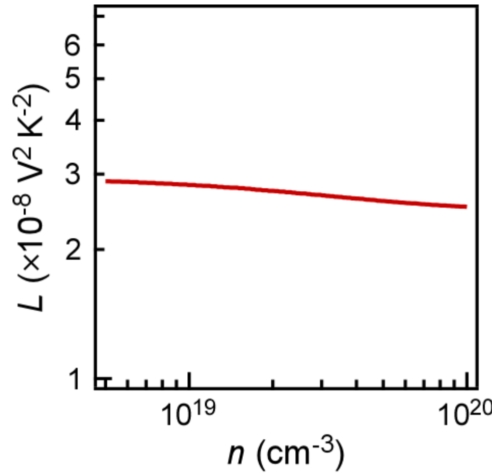

Figure S6 Calculated L as a function of n.

S6 Detail of lattice thermal conductivity calculation

The theoretical lattice thermal conductivity κ_{lat} is described on the basis of Debye-Callaway model as follows;

$$\kappa_{lat}=\frac{k_B}{2\pi^2 v}\left(\frac{k_B T}{\hbar}\right)^3 \int_0^{\theta_D/T} \tau \frac{x^4 e^x}{(e^x-1)^2} dx \quad \text{(S10)},$$

where k_B is Boltzmann constant, v is average sound velocity, $\hbar$ is reduced Planck constant, x is reduced phonon energy, θ_D is Debye temperature, and τ is the combined relaxation time of phonon. The τ^{-1} is written as $\tau^{-1}=\tau_{imp}^{-1}+\tau_{Um}^{-1}$ through Matthiessen's rule, where τ_{imp}^{-1} and τ_{Um}^{-1} are relaxation rates of impurity scattering and Umklapp scattering, respectively. According to the previous studies [8, 9], τ_{imp}^{-1} and τ_{Um}^{-1} are given by $\tau_{imp}^{-1}=(V_{av}\Gamma/4\pi v^3)(k_B T/\hbar)^4 x^4$ and $\tau_{Um}^{-1}=(k_B^2\gamma_G^2/(\hbar M_a v^2\theta_D))x^2T^3\exp(-\theta_D/(3T))$, respectively, where V_{av} is average atomic volume, γ_G is Grüneisen parameter, and M_a is average mass of the compound. The Γ is disorder parameter described as $\Gamma=\Gamma_m+\Gamma_s$, where Γ_m and Γ_s are scattering parameters due to mass and strain field fluctuations, respectively [10, 11]. Γ_m and Γ_s are calculated using the following equations:

$$\Gamma_m=\sum_i c_i \left(\frac{\overline{M_i}}{M_a}\right)^2 \Gamma_{i,m} \quad \text{(S11)},$$

$$\Gamma_{i,m}=\sum_j f_j \left(1-\frac{m_j^i}{\overline{M_i}}\right)^2 \quad \text{(S12)},$$

$$\Gamma_s=\sum_i c_i \left(\frac{\overline{r_i}}{r_a}\right)^2 \Gamma_{i,s} \quad \text{(S13)},$$

$$\Gamma_{i,s}=\sum_j f_j \left(1-\frac{r_j^i}{\overline{r_i}}\right)^2 \quad \text{(S14)},$$

where $\overline{M_i}$ ($\overline{r_i}$) is average atomic mass (size) for the ith sublattice, c_i is relative fraction for the ith sublattice, r_a is average atomic size of the compound, m_j^i (r_j^i) is the jth atomic mass (size) on the ith sublattice, and f_j is the jth atomic fraction on the ith sublattice. The theoretical κ_{lat} was calculated using these eqs (S10)-(S14) with the input parameters shown in Table S3.

Table S3 Input parameters for calculating κ_{lat} of SnO_2.

Parameters	Description	Values
v	Average sound velocity	4300 ms^{-1}
θ_D	Debye temperature	570 K
V_{av}	Average atomic volume	7.15×10^{-29} m^3
γ_G	Grüneisen parameter	0.98 (Average value of 0.79 and 1.18 [12])
m_{Sn}	Mass of Sn atom	1.97×10^{-25} kg
m_O	Mass of O atom	2.65×10^{-26} kg
m_{As}	Mass of As atom	1.24×10^{-25} kg
r_{Sn}	Radius of Sn atom	145 pm
r_O	Radius of O atom	48 pm
r_{As}	Radius of As atom	114 pm

References

[1] Yamasaka, S.; Watanabe, K.; Sakane, S.; Takeuchi, S.; Sakai, A.;Sawano, K.; Nakamura, Y. Independent Control of Electrical and Heat Conduction by Nanostructure Designing for Si-based Thermoelectric Materials. *Sci. Rep.* **2016**, 6, 22838.

[2] Sakane, S.; Ishibe, T.; Taniguchi, T.; Naruse, N.; Mera, Y.;Fujita, T.; Alam, M. M.; Sawano, K.; Mori, N.; Nakamura, Y. Thermoelectric Power Factor Enhancement based on Carrier Transport Physics in Ultimately Phonon-controlled Si Nanostructures. *Mater. Today Energy* **2019**, 13, 56−63

[3] Wei, Y.; Chen, C.; Yuan, G.; Gao, S. SnO_2 Nanocrystals with Abundant Oxygen Vacancies: Preparation and Room Temperature NO_2 Sensing. *J. Alloy Compd.* **2016**, 681, 43-49.

[4] Yang, Y.; Wang, Y.; Yin, S. Oxygen Vacancies Confined in SnO_2 Nanoparticles for Desirable Electronic Structure and Enhanced Visible Light Photocatalytic Activity. *Appl. Surf. Sci.* **2017**, 420, 399-406.

[5] Wang, Z.; Zhang, T.; Han, T.; Fei, T.; Liu, S.; Lu, G. Oxygen vacancy engineering for enhanced sensing performances: Acase of SnO2 nanoparticles-reduced graphene oxide hybrids forultrasensitive ppb-level room-temperature NO2sensing. *Sens. Actuators B* **2018**, 266, 812-822.

[6] Ishibe, T.; Tomeda, A.; Komatsubara, Y.; Kitaura, R.; Uenuma, M.; Uraoka, Y.; Yamashita, Y.; Nakamura, Y. Carrier and Phonon Transport Control by Domain Engineering for High-Performance Transparent Thin Film Thermoelectric Generator. *Appl. Phys. Lett.* **2021**, 118, 151601.

[7] Stjerna, B.; Olsson, E.; Granqvist, C. G. Optical and Electrical Properties of Radio Frequency Sputtered Tin Oxide Films Doped with Oxygen Vacancies, F, Sb, or Mo. *J. Appl. Phys.* **1994**, 76, 3797-3817.

[8] Holland, M. G. Phonon Scattering in Semiconductors from Thermal Conductivity Studies. *Phys. Rev.* **1964**, 134, A471.

[9] Heremans, J. P.; Morelli, D. T. Estimation of the Isotropic Effect on the Lattice Thermal Conductivity of Group IV and Group III-V Semiconductors. *Phys. Rev. B* **2002**, 66, 195304.

[10] Yang, J.; Meisner, G. P.; Chen, L. Strain Field Fluctuation Effects on Lattice Thermal Conductivity of ZrNiSn-Based Thermoelectric Compounds. *Appl. Phys. Lett.* **2004**, 85, 1140-1142.

[11] Li, J.; Xie, Y.; Zhang, C.; Ma, K.; Liu, F.; Ao, W.; Li, Y.; Zhang, C. Stacking Fault-Induced Minimized Lattice Thermal Conductivity in the High-Performance GeTe-Based Thermoelectric Materials upon Bi_2Te_3 Alloying. *ACS Appl. Mater. Interfaces* **2019**, 11, 20064-20072.

[12] Türkes, P.; Pluntke, Ch.; Helbig, R. Thermal Conductivity of SnO_2 Single Crystals. *J. Phys. C: Solid St. Phys.* **1980**, 13, 4941-4951.